# REPORT DOCUMENTATION PAGE

*Form Approved*
*OMB No. 0704-0188*



| **1. REPORT DATE** *(DD-MM-YYYY)* | **2. REPORT TYPE** | **3. DATES COVERED** *(From - To)* |
|---|---|---|
| 6-07-2011 | Conference paper | |

**4. TITLE AND SUBTITLE**

**Non-Intrusive, Time-Resolved Hall Thruster Near-Field Electron Temperature Measurements**

**5a. CONTRACT NUMBER**

**5b. GRANT NUMBER**

**5c. PROGRAM ELEMENT NUMBER**

**6. AUTHOR(S)**
Ashley E. Gonzales, William A. Hargus, Michael R. Nakles

**5d. PROJECT NUMBER**

**5f. WORK UNIT NUMBER**
**23080535**

**7. PERFORMING ORGANIZATION NAME(S) AND ADDRESS(ES)**

Air Force Research Laboratory (AFMC)
AFRL/RZSS
1 Ara Road
Edwards AFB CA 93524-7013

**8. PERFORMING ORGANIZATION REPORT NUMBER**

AFRL-RZ-ED-TP-2011-288

**9. SPONSORING / MONITORING AGENCY NAME(S) AND ADDRESS(ES)**

Air Force Research Laboratory (AFMC)
AFRL/RZS
5 Pollux Drive
Edwards AFB CA 93524-7048

**10. SPONSOR/MONITOR'S ACRONYM(S)**

**11. SPONSOR/MONITOR'S NUMBER(S)**
AFRL-RZ-ED-TP-2011-288

**12. DISTRIBUTION / AVAILABILITY STATEMENT**

Approved for public release; distribution unlimited (PA #11282).

**13. SUPPLEMENTARY NOTES**
For presentation at the AIAA Joint Propulsion Conference in San Diego, CA, 31 Jul – 3 Aug 2011.

**14. ABSTRACT**

With the growing interest in Hall thruster technology, comes the need to fully characterize the plasma dynamics that determine performance. Of particular interest is the existence of a periodic low frequency oscillation, commonly referred to as the breathing mode. Although there has been a significant effort to quantify plasma properties, this has been primarily limited to time-averaged measurements. In order to fully understand the periodic instabilities characteristic of Hall thruster behavior, time resolved techniques must be developed. This study presents a non-intrusive method of determining time-resolved electron temperature fluctuations during the breathing mode cycle. A triggering system was developed to synchronize measurements to thruster discharge current oscillations. Emission in the NIR is measured near the thruster exit plane using an optical fiber coupled to a 1.25 m focal length spectrometer and intensified CCD (ICCD) detector. ICCD gating is controlled using the output of the triggering system and a user controlled gate delay. This allows emission sampling only from the desired portion of the breathing mode cycle. Emission is integrated over several periods to allow for improved signal to noise ratio (SNR). Electron temperature is determined using the intensity of Xe I emission lines in the context of a collisional-radiative model. The resulting measured electron temperature fluctuations during a nominal breathing mode cycle are presented for a 600 W Hall effect thruster at a single nominal operating condition.

**15. SUBJECT TERMS**

| **16. SECURITY CLASSIFICATION OF:** | | | **17. LIMITATION OF ABSTRACT** | **18. NUMBER OF PAGES** | **19a. NAME OF RESPONSIBLE PERSON** |
|---|---|---|---|---|---|
| | | | | | Dr. William A. Hargus, Jr. |
| **a. REPORT** | **b. ABSTRACT** | **c. THIS PAGE** | SAR | 31 | **19b. TELEPHONE NUMBER** *(include area code)* |
| **Unclassified** | **Unclassified** | **Unclassified** | | | N/A |

AIAA Joint Propulsion Conference
31 July-3 Aug 2011
San Diego, CA

# Non-Intrusive, Time-Resolved Hall Thruster Near-Field Electron Temperature Measurements

Ashley E. Gonzales
Air Force Research Laboratory
Edwards AFB, CA 93524

William A. Hargus, Jr.
Air Force Research Laboratory
Edwards AFB, CA 93524

Michael R. Nakles
E.R.C. Inc.
Edwards AFB, CA 93524

## Abstract

With the growing interest in Hall thruster technology, comes the need to fully characterize the plasma dynamics that determine performance. Of particular interest is the existence of a periodic low frequency oscillation, commonly referred to as the breathing mode. Although there has been a significant effort to quantify plasma properties, this has been primarily limited to time-averaged measurements. In order to fully understand the periodic instabilities characteristic of Hall thruster behavior, time resolved techniques must be developed. This study presents a non-intrusive method of determining time-resolved electron temperature fluctuations during the breathing mode cycle. A triggering system was developed to synchronize measurements to thruster discharge current oscillations. Emission in the NIR is measured near the thruster exit plane using an optical fiber coupled to a 1.25 m focal length spectrometer and intensified CCD (ICCD) detector. ICCD gating is controlled using the output of the triggering system and a user controlled gate delay. This allows emission sampling only from the desired portion of the breathing mode cycle. Emission is integrated over several periods to allow for improved signal to noise ratio (SNR). Electron temperature is determined using the intensity of Xe I emission lines in the context of a collisional-radiative model. The resulting measured electron temperature fluctuations during a nominal breathing mode cycle are presented for a 600 W Hall effect thruster at a single nominal operating condition.

## Introduction

Hall thrusters are becoming widely used for spacecraft station-keeping due to their low thrust, high specific impulse operation. Despite their higher system complexity relative to conventional monopropellant chemical thrusters, the significant reduction of station-keeping propellant (by as much as 10x for north-south station-keeping of a geosynchronous spacecraft) makes this technology economically advantageous. While a number of Hall effect thrusters are now space qualified, there is a strong research component actively pursuing the extension of this spacecraft propulsion technology for higher powers, longer life, and new propellants. These research efforts have developed a number of diagnostics and models that presently provide an adequate understanding of the time averaged plasma dynamics which govern critical processes such as scaling, sputter induced erosion, and propellant utilization. However, while it is known that periodic plasma instabilities (10's of kHz through MHz) strongly affect the plasma electron transport within the discharges of Hall effect thrusters, models and experiments have for the most part not measured these phenomena quantitatively. This paper examines preliminary measurements of electron temperature using emission spectroscopy with time resolutions of 1 μs over a periodic 15 kHz ionization wave in the near-field of a medium power Hall effect thruster.

The most often studied periodic plasma instability of a Hall effect thruster is the low frequency (10-50 kHz) fluctuation in discharge current, often referred to in the literature as the *breathing mode*. The Hall thruster breathing mode can be seen both experimentally and through numerical modeling[1,2]. The oscillations are believed to be due to a cycling of the neutral and plasma density in the exhaust region. The neutrals fill the exhaust region and are quickly ionized due to the local high electron temperature. The neutral population is depleted and the ionization wave moves towards the anode. The neutral flow front moves upstream where there is a lower ionization rate. Without neutrals to ionize, the plasma density in the exhaust decreases resulting in lower electron influx. The neutrals then refill the exhaust region, and the cycle begins again. This plasma oscillation has also been called the *neutral transit time instability*, as the period may be approximated by the acceleration channel length divided by the neutral propellant thermal velocity. However, the frequency is also dependant on other properties such as the magnetic field strength, discharge potential, and plasma density.

Emission spectroscopy diagnostics are valuable tools at characterizing plasma parameters, such as electron temperature. While electron temperature has previously been measured using various electrostatic probes [3,4], such measurements are intrusive and have inherent limitations with regard to time-resolution. Optical emission measurements have the potential to resolve time scales on the ns temporal scale, or lower, are mainly limited by SNR. Additionally, optical measurements provide access to the thruster near-field, unlike probes which are limited due to their interference with the plume. Emission diagnostics therefore present an obvious choice for the development of time resolved plasma diagnostics at μs or higher temporal resolutions.

The purpose of this work is to demonstrate the capabilities of such emission diagnostics through time-resolved measurements of electron temperature during the breathing mode cycle in a medium power Hall effect thruster near-plume. This study uses NIR xenon neutral emission measurements in conjunction with a collisional-radiative model to infer electron temperature. Relying on the highly periodic nature of the oscillations, a portion of the 30μs period is measured with 1μs integration time and accumulated over several periods to achieve adequate SNR. Repeating this process during the period of the breathing mode, and assuming phase synchronicity, allows us to measure the emission temporal behavior over a representative period. Therefore, the measurements are time accurate and the plasma oscillation periodicity allows us to make estimations of the periodicity of the electron temperature variation.

## Collisional-Radiative Model

### Theory

A collisional-radiative model (CRM) is used to relate observed emission to plasma parameters. A CRM uses primary excitation and deexcitation mechanisms to predict emission as a function of plasma conditions. Initial simplified efforts in modeling the Hall thruster plasma emission were done using a corona model [5]. The corona model simplifies the plasma by assuming excitation due only to electronic collisions and deexcitation due only to radiative decay. One difficulty with this model is the lack of heavy particle collisions. Although electron collisions happen at a much higher frequency, it has been shown that heavy particle collisions should not be assumed negligible for Hall thruster plasma conditions [6].

Another shortcoming of the corona model is that it does not account for the presence of Xe metastable states. Metastable states are energy levels that remain populated for long time scales due to a lack of allowed radiative decay transitions, and therefore collisions with this metastable state must be taken into account. A simplified view of the Xe energy level diagram with a number of radiative transitions of interest is shown in Figure 1 (a). The $1s_5$ metastable state is populated from radiative decay from the $2p_i$ series but has no allowable radiative decay path to ground. The main mechanism for leaving this energy level is collisional excitation. Therefore this state remains populated for longer timescales.

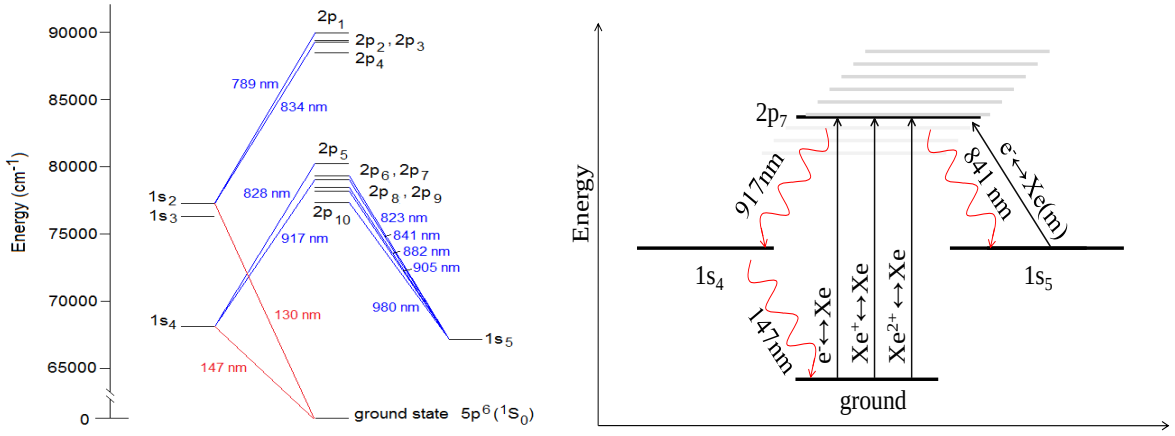


Figure 1: (a) Simplified Neutral Xenon Energy Level Diagram and allowable radiative decay pathways; (b) KCD excitation and deexcitation pathways including metastable (1s5) state and heavy particle collisions with ground state

The KCD collisional-radiative model used in this study was developed by Karabadzhak et al[7] based on the collision cross-sections developed by Chui[8] and Sommerville[9]. A schematic of the KCD model is shown in Figure 1 (b). The KCD model builds on the corona model by including heavy particle and metastable collisions, assumed exclusively with electrons. The $2p_i$ series is simplified by assuming only two possible radiative pathways: radiative decay to ground through the $1s_4$ state, or decay to the metastable $1s_5$ state. Metastables are modeled assuming steady state equilibrium between metastables gained through collisional excitation from ground to the $2p_i$ series followed by radiative decay to $1s_5$, and metastables lost through collisional excitation from the metastable state followed by radiative decay to $1s_4$.

The primary mechanisms considered for the neutral Xe emission are as follows:

$$e^- + Xe \rightarrow Xe^* + e^- \quad a)$$
$$e^- + Xe_m \rightarrow Xe^* + e^- \quad b)$$
$$Xe^+ + Xe \rightarrow Xe^* + Xe^{+*} \quad c)$$
$$Xe^{2+} + Xe \rightarrow Xe^* + Xe^{2+*} \quad d)$$

The radiation intensity per unit volume can then be approximated using

$$J_{XeI}(\lambda) = \frac{\hbar c}{4\pi\lambda}\left[N_0 N_e k_{eO}^{\lambda} + N_m N_e k_{em}^{\lambda} + N_0 N_1 k_{10}^{\lambda} + N_0 N_2 k_{20}^{\lambda}\right] \quad (1)$$

where $N_i$ are the species number densities; $k_{eO}^{\lambda}$ is the excitation rate coefficient for electrons with neutrals with emission at wavelength λ; $k_{em}^{\lambda}$ is the emission excitation rate coefficient for electrons with metastables; and $k_{10}^{\lambda}$ and $k_{20}^{\lambda}$ are the emission excitation rate coefficient for $Xe^+$ and $Xe^{+2}$ ions with neutrals. Assuming quasineutrality, $N_e = N_1 + 2N_2$, and substituting $\alpha = N_1/N_e$ , Equation (1) can be rewritten as

$$J_{XeI}(\lambda) = \frac{\hbar c}{4\pi\lambda}(N_0 N_e)\left[k_{eO}^{\lambda} + \frac{N_m}{N_0} k_{em}^{\lambda} + \alpha\, k_{10}^{\lambda} + \frac{1-\alpha}{2} k_{20}^{\lambda}\right] \quad (2)$$

Rate coefficients are determined using

$$k_{ij}^{\lambda} = \int_0^{\infty} f_i(E_i)\sigma_{ij}^{\lambda}(E_i)u_i\, dE_i \quad (3)$$

where $f_i(E_i)$ is the energy distribution of species i; $\sigma_{ij}^{\lambda}(E_i)$ is the excitation cross sections for a particle i, with energy $E_i$, with a particle j to produce emission at λ ; and $u_i$ is the velocity of particle i. Excitation cross sections for neutral-electron and neutral-ion collisions are determined empirically from Chiu[8] and Sommerville[9]. Assuming a Maxwellian electron energy distribution, $k_{eO}^{\lambda}$ is determined as a function of the electron temperature, Te. Rate coefficients $k_{1O}^{\lambda}$ and $k_{2O}^{\lambda}$ are determined assuming a uniform ion energy distribution. Cross sections for electron-metastable collisions have yet to be determined empirically. Therefore the excitation rate coefficient $k_{em}^{\lambda}$is then approximated using the upper $2p_i$ level degeneracy and branching probabilities.

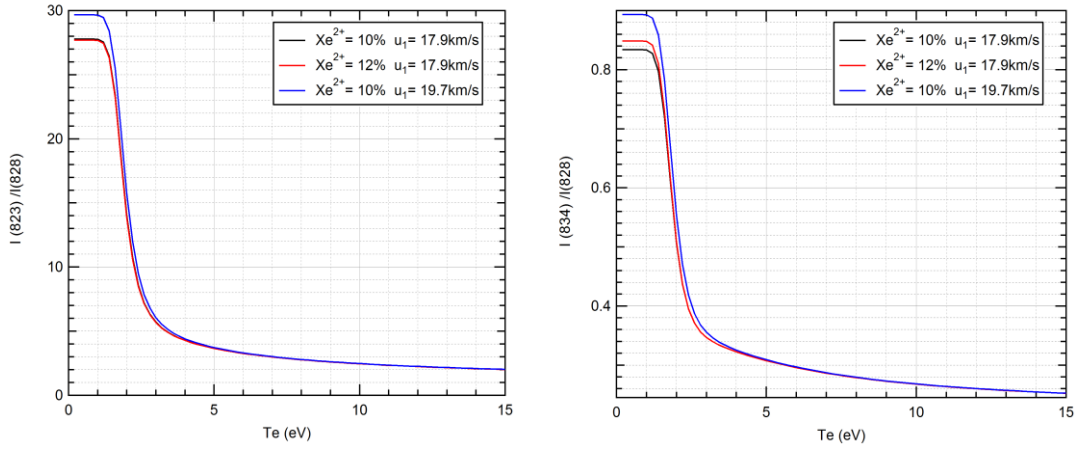


Figure 2: Calculated intensity ratios as a function of electron temperature using empirical data for ion relative population and velocity in comparison to a 20% increase in $Xe^{2+}$ population and a 10% increase in ion velocity

Intensity ratios for the $I_{823}/I_{828}$ and $I_{834}/I_{828}$ calculated using the KCD model are shown in Figure 2. Ion species populations input into the model are from probe measurements by Nakles et al[10] and Ekholm et al[11] and ion velocity inputs are based on data from Nakles et al[12]. A parameter variation comparison was done using a 20% increase in the $Xe^{2+}$ population and a 10% increase in the ion velocity to determine their influence on the model. Both models showed little sensitivity to the relative species populations or ion velocity, except in the low electron temperature regions where ion collisions play a more significant role. The $I_{834}/I_{828}$ line is more accurately modeled than the $I_{823}/I_{828}$ line ratio, which relies on the metastable approximations for $I_{823}$ line, but the $I_{834}/I_{828}$ method shows higher sensitivity to intensity ratio in the 5-10 eV region, making it more susceptible to temperature error due to uncertainties in line intensity. A 5% uncertainty in the line ratio in the 5-10 eV region results in a 1 eV uncertainty for the $I_{823}/I_{828}$ and a 2 eV uncertainty in the $I_{834}/I_{828}$ method. The lower emission signal of the $I_{834}$ line also makes this method more difficult to accurately determine intensity ratios in low signal to noise ratio conditions, leading to higher temperature uncertainties.

## Experimental Apparatus

### Test Facility and Hall Effect Thruster

The measurements reported here were performed in vacuum Chamber 1 at the Air Force Research Laboratory at Edwards Air Force Base. This vacuum facility consists of a 2.4 m diameter, 4.1 m long cylindrical, non-magnetic stainless steel vacuum chamber with two liquid nitrogen baffled (76 K), 1.2 m flanged gaseous helium two stage cryogenic (15 K) vacuum pumps capable of pumping speeds of 48,500 L/s on xenon. A cold cathode gauge is used to determine a chamber background pressure of approximately $4 \times 10^{-6}$ Torr (corrected for xenon) during thruster operation.

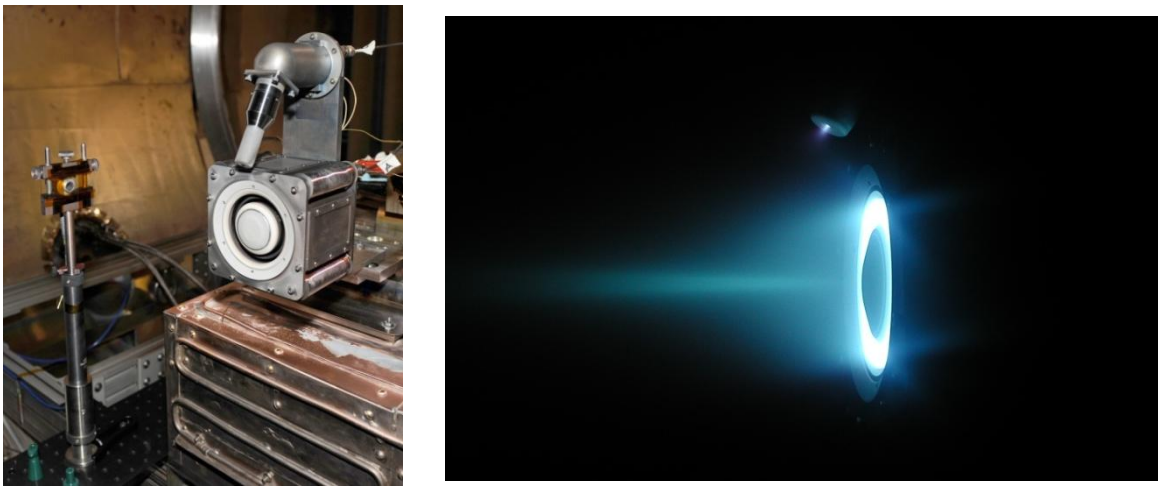

Figure 3: Photographs of BHT-600 Hall effect thruster. Left: Thruster shown with optical collection apparatus mounted to left. Collection volume taken 6 mm downstream of exit plane. Right: Thruster firing with Xe propellant, highlighting structure of near plume.

The Hall effect thruster used in this study is a, 600 W BHT-600 with a 3.2 mm hollow cathode manufactured by the Busek Company (Natick, MA) This thruster has been studied previously using both electrostatic probes and various optical diagnostics[10, 11,12,13,14,15]. Photographs of the Chamber 1 apparatus

and thruster firing are shown in Figure 3. The BHT-600 Hall effect thruster has an acceleration channel outer radius of 32 mm, an inner radius of 24 mm, and a 10 mm depth. The magnetic field is produced by four outer coils, and one inner magnetic coil. The outer and inner coils are independently addressable for optimization of the field strength. The nominal conditions and performance of the BHT-600 as provided by the Busek Company are shown in Table 1.

At nominal conditions the BHT-600 produces consistent, periodic 40 kHz oscillations. A sample thruster discharge current measurement is shown in Figure 4. Although the amplitude of the signal varies, the period of the fluctuations remains consistent at 26.4± 0.3 μs based on the half width at half maximum (HWHM) of the FFT trace. This repeatability is what allows for shots to be accumulated at the same position in the fluctuation over many periods. Discretizing the current fluctuation into 1μs sections, this accumulation method can be done at each temporal position in the oscillation.

Table 1: BHT-600 Hall thruster at nominal xenon operating conditions and performance

| Parameter | Value |
|---|---|
| Anode Flow Rate | 2.45 mg/s |
| Cathode Flow Rate | 197 μg/s |
| Anode Potential | 300 V |
| Anode Current | 2.05 A |
| Magnetic Current (inner coils) | 2.0 A |
| Magnetic Current (outer coils) | 2.0 A |
| Thrust | 42 mN |
| Specific Impulse | 1650 s |
| Anode Efficiency | 55.0% |

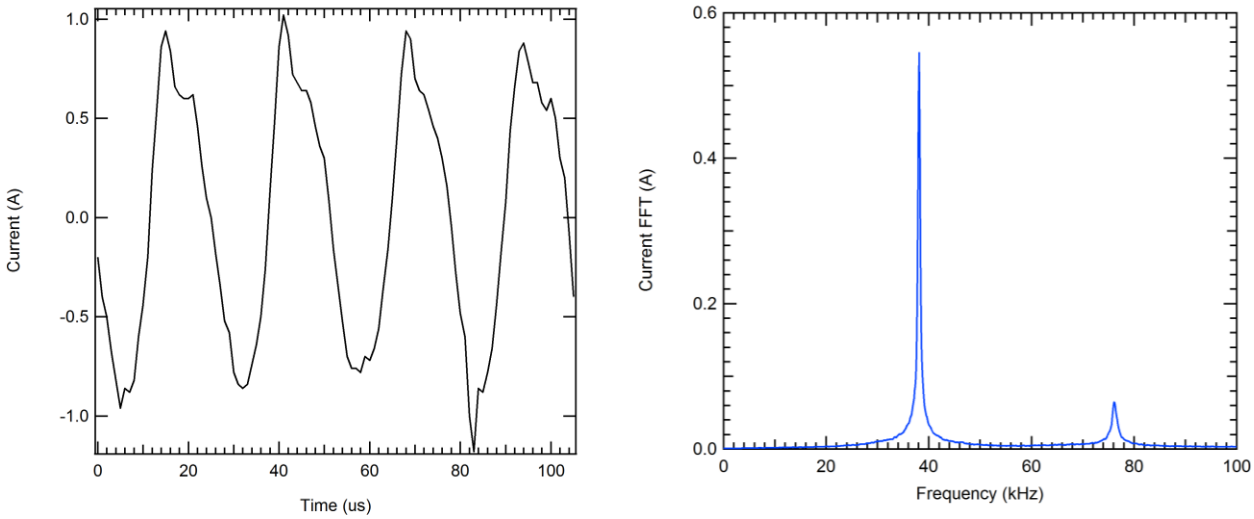


Figure 4: Typical BHT-600 breathing mode discharge current oscillations at nominal conditions. Left: thruster current oscillations at approximately 26 μs. Right: current FFT trace with oscillation frequency peak at 38 kHz.

**Timing and Triggering Circuit**

The temporal resolution of the data was achieved using a triggering system to synchronize the ICCD gating with discharge current oscillations. A schematic layout of the timing circuit constructed for these measurements is shown in Figure 5. The trigger circuit uses analog components to process the discharge current signal into a transistor-transistor logic (TTL) output, which is used to synchronize camera gating to the current oscillations. Thruster current oscillations are measured using a passive inductive probe, which also incidentally acts as a band pass filter (3 dB points of 120 Hz and 20 MHz with < 1° phase shift at frequencies between 1-100 kHz). This low-level voltage signal is then passed through a low pass filter and subsequently differentiated, so that the zero crossings of the differentiated signal correspond to minima in the thruster anode current signal. Using a high-speed comparator acting as a zero crossing detector, a TTL signal is produced at the minimum of the signal. A digital delay generator (DDG) is then used as a buffer between the triggering circuit and ICCD by not passing any false triggers caused by occasional inflection points in the discharge current. The result is a TTL signal synchronized with the discharge current oscillations.

Camera gating is controlled using the TTL trigger and user defined gate width and gate delay (down to ns timescale). The camera is triggered using the TTL output of the DDG, waits the specified gate delay, and then allows emission to fall on the detector for the specified gate width. This timing system allows the camera to gate at the desired temporal location over several periods and accumulate signal over the camera exposure time. The camera produces a gate monitor TTL output to ensure gating is correctly synchronized to the desired portion of the signal. A 1 GS/s oscilloscope was used to monitor the thruster discharge current, the DDG trigger output, and the ICCD gate monitor output to ensure repeatable triggering and gating.

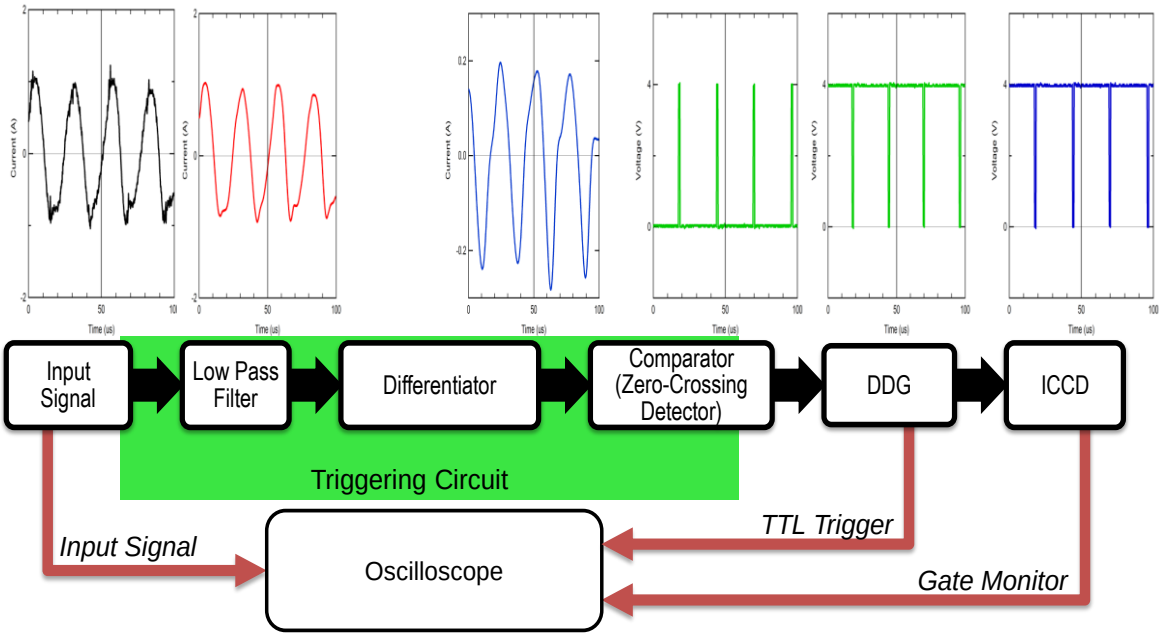


Figure 5: Data acquisition timing system schematic

**Optics**

The optical system used to measure the emission spectrum is schematically shown in Figure 6. Plume emission is collected at a single location 6 mm downstream of the thruster exit plane using a 6 mm reflective fiber optic beam coupler. The beam coupler focuses a 6 mm diameter beam onto the optical fiber. The coupler has greater than 97.5% reflectance in the 450 nm-2μm range. The 200 μm optical fibers has a numerical aperture (NA) of 0.22 and low attenuation in the NIR. To protect the optical coupler from redeposition of sputtered material, a disposable protective 1 mm thick quartz window is placed over the optical coupler aperture.

The NIR optimized fiber optic patch cord from the optical coupler connects to a fiber optic vacuum feed through the chamber wall to a second patch cord coupled to the Horiba 1250M Series II spectrometer using a Horiba fiber optic adapter. The fiber adapter uses 100 mm and 30 mm lenses to focus light emitted from the fiber onto the spectrometer entrance slit. The spectrometer, with a 1.25 m focal length (f/9), contains a 300 G/mm classically ruled diffraction grating, blazed at 500 nm, that produces a dispersion of 2.6 nm/mm. For the measurements presented here, the spectrometer entrance slit was fixed at 200 μm. While this limited the spectral resolution, it increased throughput for greater signal strength.

The desired spectrum is detected using a cooled Andor iStar® Intensified CCD (ICCD) with 1024 x 1024 pixels (13 μm x 13 μm) capable of dark currents as low as 0.065 $e^-$/pix/s. The camera intensifier system acts as a fast solid-state shutter capable of gating on 1 ns time scales. Gating is controlled by the TTL input and user defined gate delay and gate width. The individual gated shots are then accumulated over the length of the desired exposure and recorded using the National Instruments LabView PC based data acquisition system.

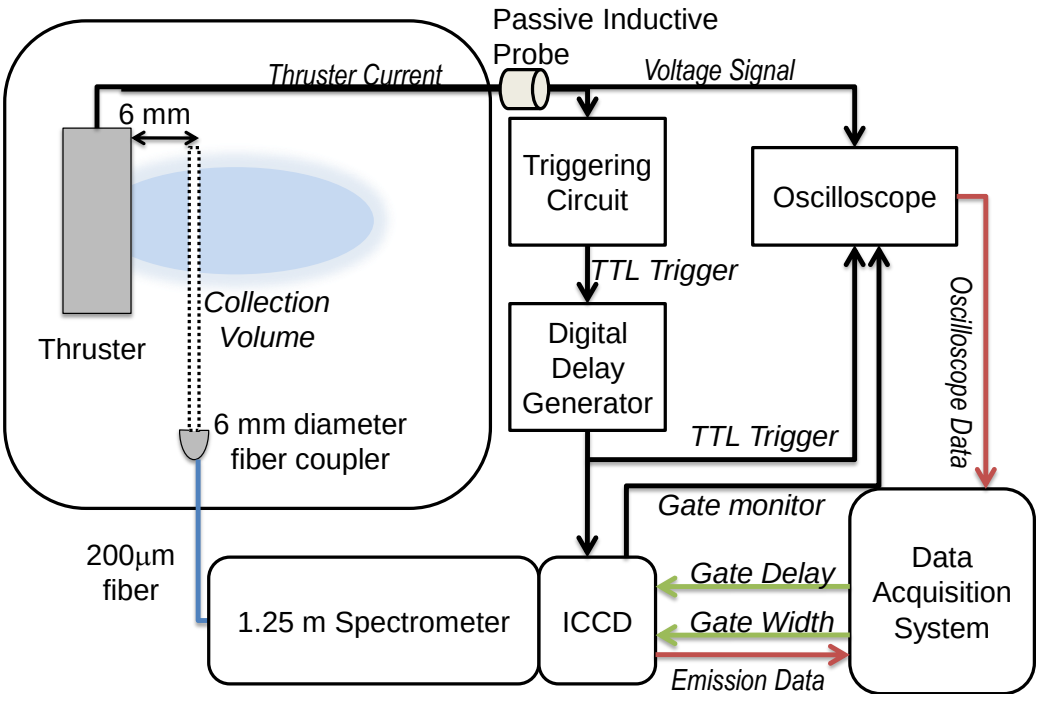


Figure 6: Optical system used to measure thruster emission using a 1.25m Horiba spectrometer with attached Andor ICCD. Emission measurements are triggered using a custom triggering circuit to synchronize measurements to current oscillations. Full breathing mode cycle is characterized by varying the inputted delay between trigger and ICC gating.

Each component of the optical system introduces a wavelength dependence on transmission. To correct for this detection wavelength dependence, a calibration was performed using a NIST traceable 200 W tungsten filament standard of spectral irradiance. The measured grey body emission is compared with the expected response to determine the relative spectral response (RSR) of the system. The average RSR is then used to correct the measured thruster emission.

## Results and Discussion

### Timing/Trigger Circuit Verification

The timing system demonstrated repeatable current synchronized triggering capabilities. A sample oscilloscope trace is shown in Figure 7. The 2 μs delay between the minimum of the current signal and the fall of the triggering circuit TTL is caused by the delays added by the active circuit components and was found to be consistent in all measurements. The ICCD is triggered after the initial TTL drop at time $t$ = 9 μs and delays gating until $t$ = 22 μs based on the 13 μs input gate delay. Additional delay added by ICCD electronics was found to be on the order of nanoseconds. After gating for 1μs, the camera waits for the next TTL trigger to start the next cycle. Signal is accumulated from each gating on the ICCD until the end of the 0.5 s exposure. Measurements of the full breathing mode cycle are achieved by varying the gate delay from 0-27 μs. Time zero shown in subsequent figures will be defined at the fall of the triggering circuit TTL, corresponding to an input gate delay of zero. Delays in gating from the ICCD electronics will be assumed negligible. A ± 0.2 μs uncertainty in the temporal resolution will be used based on the HWHM of the current FFT.

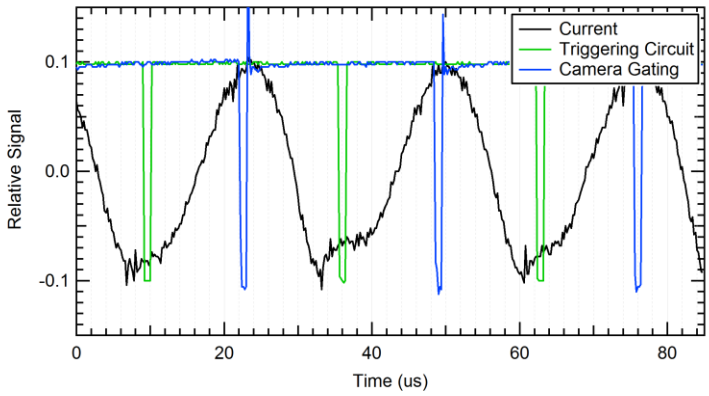


Figure 7: Sample oscilloscope trace with ICCD settings: 1 μs pulse width, 13 μs gate delay. Only 80μs of the 0.5 s exposure is shown.

### Emission Measurements

A total of 108 emission measurements were taken at nominal thruster conditions. The cooled ICCD achieved a high signal to noise ratio (SNR > 24 dB) for most cases. Emission measurements near minimum of the discharge current were difficult due to the low signal (SNR = 1.9 dB). Measurements were taken at gate widths of 1 μs with gated shots accumulated over 0.5 s exposures. The background was subtracted from the raw signal and the resulting signal was then corrected with the average RSR. A sample emission spectrum is shown in Figure 8. A majority of the measured lines in this wavelength region are strong neutral lines. The emission from the metastable linked 823 nm line is the strongest of the three lines. The metastable state allows for excited neutrals with long lifetimes, which can then be

easily re-excited producing strong emission lines. Additional neutral Xe lines seen can be seen at 820 nm and 827 nm, but their low signal in proximity to the stronger lines makes them difficult to use for diagnostic purposes. This study focuses on the use of the three strongest lines (823, 828, and 834 nm) for determination of electron temperature.

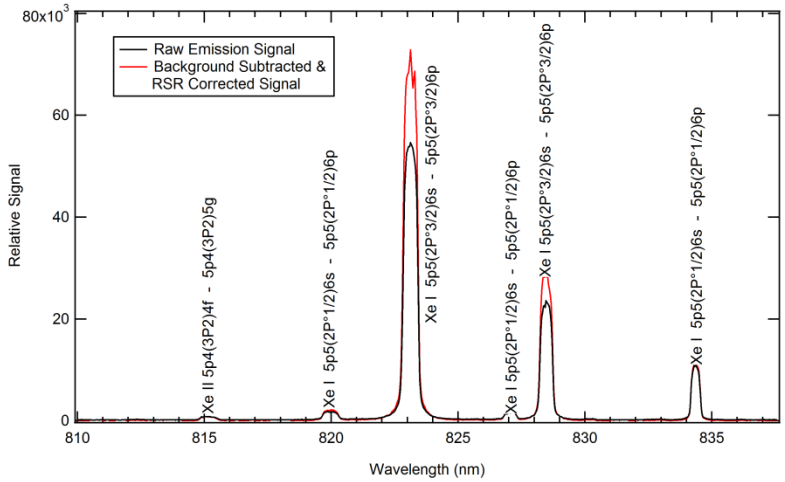


Figure 8: Sample emission spectrum of a BHT-600 at nominal operating conditions. Measurement taken near peak of discharge current oscillation with 1 μs gated shots over a 0.5 s exposure (19,000 cycles).

The peak value normalized line intensities are shown in Figure 9 with a representative current trace. There is a strong correlation between the peak of the discharge current and the peak of the Xe neutral emission. Similar results were seen in a 200 W Hall thruster study by Liu et al[16] using high speed imaging to measure oscillations in visible emission with discharge current. A 2 μs delay can be seen between the peak of the normalized intensity and the peak in the discharge current. Assuming this delay is based on the electron transit time between the measurement volume and the anode, an 8 km/s average axial electron velocity can be approximated. This is in approximate agreement with HPHall modeling which predicts a 5-10 km/s electron axial velocity between the anode and exit[17]. A significant drop in emission signal is seen after 23 μs, near the minimum of the discharge current. The low signal in this portion of the cycle increased the uncertainty in measurements, especially for the lowest intensity line at 834 nm.

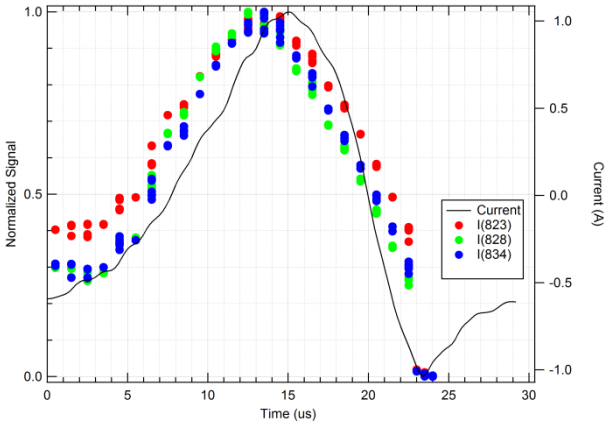


Figure 9: Normalized Xe I line intensities in comparison to discharge current. Measurements taken 6 mm downstream of thruster exit plane at nominal operating conditions. Due to low signal towards the end of the cycle, line intensities were unable to be determined due to low signal strengths.

**Electron Temperature**

Electron temperatures are determined using $I_{823}/I_{828}$ and $I_{834}/I_{828}$ line intensity ratios in conjunction with the results of the KCD model. The resulting electron temperatures are shown in Figure 10. The $I_{823}/I_{828}$ method results in electron temperatures oscillating between approximately 3 and 7 eV, peaking approximately 3 μs before the peak in discharge current. The $I_{834}/I_{828}$ method results in larger electron temperatures fluctuations (3-10 eV) peaking approximately 6 μs before the peak in discharge current. Higher scatter in the $I_{834}/I_{828}$ method versus the $I_{823}/I_{828}$ method is due to the $I_{834}/I_{828}$ method's higher sensitivity to uncertainties in line ratio. Low signal at the end of the cycle (> 22 μs) lead to higher uncertainties with the integrated line intensity for all three lines, and therefore resulted in a higher uncertainty for both temperature methods.

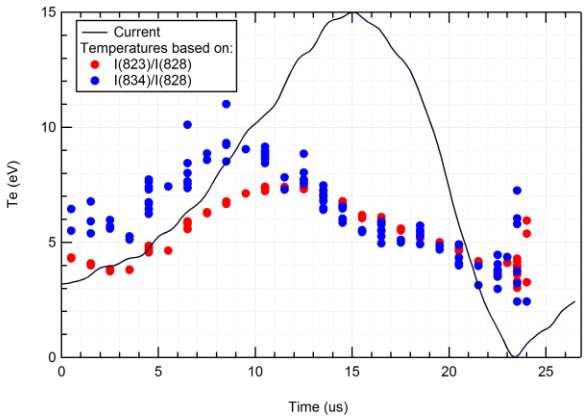


Figure 10: Temporally resolved electron temperature fluctuations measured 6 mm downstream of BHT-600 thruster exit plane at nominal operating conditions. Temperatures are determined using the KCD model a two-line emission method.

Fluctuations in electron temperature are due to competing plasma parameters that are varying during the breathing mode cycle. Fluctuations in electron heating are expected based on electric field oscillations predicted by breathing mode models[2]. Additionally, changes in density will result in temporally varying electron collisional cooling. Due to the system complexities, additional modeling work is needed to determine which of these mechanisms is primarily responsible for the 3-6 μs delay between discharge current and electron temperature.

Also of note is the 2-3 eV disagreement between the two methods for the first portion of the breathing mode cycle. One possible reason for the disagreement is the reliance on the model's metastable approximations by the $I_{834}$ line. The low electron density, low electron temperature segment of the breathing mode may not have sufficient collisions to maintain the models metastable equilibrium approximation. Another possible explanation for this disagreement is an initial non-Maxwellian electron energy distribution due to an insufficient number of electron-electron collisions. Once the collisional frequency increases with increasing plasma density, the electrons return to a Maxwellian velocity distribution and are equilibrated by the increase in collisions.

Experiments to temporally resolve plasma behaviors were also performed by Lobbia et al. using a high-speed dual Langmuir probe[3]. Using rapid sweeping, this probe is able to measure electron density, electron temperature, and plasma potential with a 10 μs temporal resolution. Electron temperature and plasma potential measurements of the far field (20 cm downstream) of a 600W thruster are found to be nearly in phase with discharge current. However the 3-6 μs shift seen in our measurements is considerably under the temporal resolution of the high-speed dual Langmuir probe method.

## Conclusions

A novel, non-intrusive method for time-resolved (1μs) electron temperature measurement has been presented using emission spectroscopy and the KCD model. An analog triggering system was developed to synchronize ICCD gated emission measurements with the desired portion of the discharge current oscillation period. Measurements were taken by integrating the gated emission signal over several cycles, producing high signal to noise ratio measurements. The Xe I NIR emission fluctuations were observed to be nearly in phase with discharge current oscillations. Electron temperature fluctuations (approximately 3-10 eV) were found to be 3-6 μs out of phase with discharge current oscillations. Temperature disagreements between the $I_{823}$ /$I_{828}$ and $I_{834}$ /$I_{828}$ methods in the beginning of the cycle may suggest an initial non-Maxwellian electron energy distribution or weaknesses in the modeling at the low Te, low electron density portion of the cycle.

Future experiments will focus on achieving spatial and temporal resolution as well as expanding measurements to other plasma properties. Spatial resolution can be achieved utilizing the inversion method presented by Matlock et al[18] in which radial emission sweeps can be used to determine a three-dimensional estimate of the electron temperature. Additionally, this optical system can be used to ascertain other time-resolved plasma properties, such as ion velocity using Doppler shift. The development of these nonintrusive temporally and spatially resolved diagnostics is vital to fully understanding the plasma dynamics governing the Hall thruster breathing mode.

## Acknowledgements

The authors would like to thank Dr. Mike Holmes and Mr. Paul Adkison for their assistance with the development of the triggering circuit. Their practical knowledge greatly assisted in its development. Thanks are also due to Dr. Michelle Scharfe and Dr. Justin Koo for their helpful discussions and assistance with the implementation of the collisional-radiative model.

---

## References

[1] Boeuf, J. P.; Garrigues, L. , "Low frequency oscillations in a stationary plasma thruster," *Journal of Applied Physics* , vol.84, no.7, pp.3541-3554, Oct 1998.
[2] Choueiri, E. Y. ,"Plasma oscillations in hall thrusters," *Physics of Plasmas*, vol. 8, no. 4, pp. 1411–1426, April 2001.
[3] Lobbia, RB and Gallimore, A.D. "High-speed dual Langmuir probe," *Rev. Sci. Instrum*. 81, 073503, 2010.
[4] Beal, Brian; Gallimore, Alec; Hargus, William, "Preliminary Plume Characterization of a Low-Power Hall Thruster Cluster" *38th AIAA/ASME/SAE/ASEE Joint Propulsion Conference and Exhibit, Indianapolis, Indiana*, AIAA-2002-4251, 2002.
[5] Griem, H. Plasma Spectroscopy New York: McGraw-Hill, 1964.
[6] Karabadzhak, George F.; Chiu, Yu-hui; Williams, S., Dressler, Rainer A, *37th AIAA/ASME/SAE/ASEE Joint Propulsion Conference and Exhibit, Salt LakeCity, UT*, AIAA-2001-3893, 2001
[7] Karabadzhak, George F.; Chiu, Yu-hui; Dressler, Rainer A.; , "Passive optical diagnostic of Xe propelled Hall thrusters. II. Collisional-radiative model," *Journal of Applied Physics* , vol.99, no.11, pp.113305-113305-12, Jun 2006

[8] Chiu, Yu-hui; Austin, Brad L.; Williams, Skip; Dressler, Rainer A.; Karabadzhak, George F.; , "Passive optical diagnostic of Xe-propelled Hall thrusters. I. Emission cross sections," *Journal of Applied Physics* , vol.99, no.11, pp.113304-113304-11, Jun 2006

[9] Sommerville, Jason D. ; King, Lyon B. ; Chiu, Yu-Hui ; Dressler, Rainer A ,"Ion-Collision Emission Excitation Cross Sections for Xenon Electric Thruster Plasmas," *Journal of Propulsion and Power,* 24, 880, 2008

[10] Nakles, Michael R; Barry, Ryne R; Larson, C W; Hargus, Jr, William A "A Plume Comparison of Xenon and Krypton Propellant on a 600W Hall Thruster" *31st International Electric Propulsion Conference, Ann Arbor, MI* , 2009.

[11] Ekholm, Jared M.; Hargus, Jr., William A.; Larson, C. W.; Nakles, Michael R.; Reed, Garrett; Niemela, Carrie S, " Plume characteristics of the Busek 600 W Hall Thruster," *42nd AIAA/ASME/SAE/ASEE Joint Propulsion Conference & Exhibit, Sacramento, California,* AIAA 2006-4659, 2006.

[12] Nakles, Michael R; Hargus, Jr, William A, "Background Pressure Effects on Internal and Near-field Ion Velocity Distribution of the BHT-600 Hall Thruster, " *44th AIAA/ASME/SAE/ASEE Joint Propulsion Conference & Exhibit, Hartford, Conneticut*, 2008.

[13] Niemela, Carrie S. ; Cheng, Shannon Y. ; Brieda, Lubos ; Nakles, Michael ; Ekholm, Jared ; Hargus, Jr., William, "Comparison of Hall Thruster Plume Expansion Model with Experimental Data," *42nd AIAA/ASME/SAE/ASEE Joint Propulsion Conference & Exhibit, Sacramento, California,* 2006.

[14] Victor, Allen; Zurbuchen, Thomas; Gallimore, Alec, "Ion-Energy Plume Diagnostics on the BHT-600 Hall Thruster Cluster," *Journal of Propulsion and Power*, vol.22 no.6 (1421-1424), 2006.

[15] Hargus, Jr, William A; Charles, Christopher S "Near Plume Laser Induced Fluorescence Velocity Measurements of a 600 W Hall Thruster," *44th AIAA/ASME/SAE/ASEE Joint Propulsion Conference & Exhibit, Hartford, Conneticut*, 2008.

[16] Liu, David; Huffman, Richard E., Branam, Richard D.; Hargus, Jr, William A, "Ultra-High Speed Imagining of Hall Thruster Discharge Oscillation with Krypton Propellant," *IEEE T. Plasma. Sci.*, (in press).

[17] Scharfe, Michelle K, Koo, Justin W, personal communication, 2011.

[18] Matlock, Taylor S. ; Larson, C. W. ; Hargus, Jr, William A; Nakles, Michael R., "An Inversion Method for Reconstructing Hall Thruster Plume Parameters from Line Integrated Measurements," *43rd AIAA/ASME/SAE/ASEE Joint Propulsion Conference and Exhibit, Cincinnati, OH,* 2007.


# Non-Intrusive, Time-Resolved Hall Thruster Near-Field Electron Temperature Measurements

**Ashley E. Gonzales, AFRL**

**William A. Hargus, Jr., AFRL**

**Michael R. Nakles, E.R.C. Inc.**

**Edwards AFB, CA**

# Background: Diagnostics

## Probe

- Measurements
  - Langmuir- $T_e$, density, $e^-$ EDF
  - RPA – ion EDF
  - Faraday- thruster beam current
- Intrusive- spatially limited
- Temporally limited due to sweeps
  - Lobbia[1] (10 μs resolution)

[1] Lobbia, RB and Gallimore, A.D. , *Rev. Sci. Instrum*. 81, 073503, 2010

## Emission

- Measurements
  - Line Intensity ratio- $T_e$
  - Absolute Intensity - Density
  - Doppler Shift - velocity
- Non-intrusive- capable of near field measurements
- Line of sight averaging
- Measurements on ns timescales

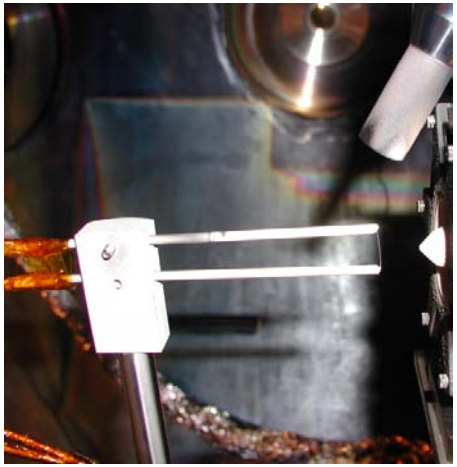

**Langmuir (Cold emissive) Probe**

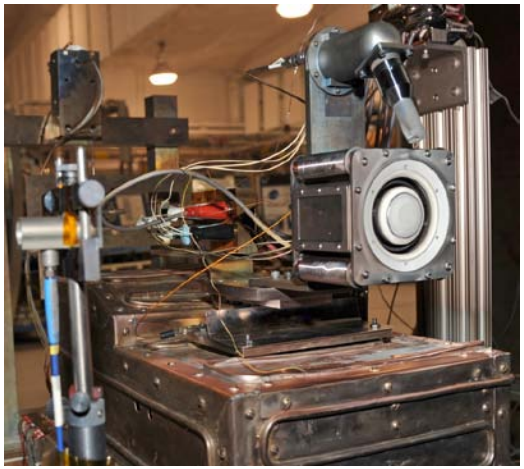

**Emission Beam Coupler**

# Background: Breathing Mode

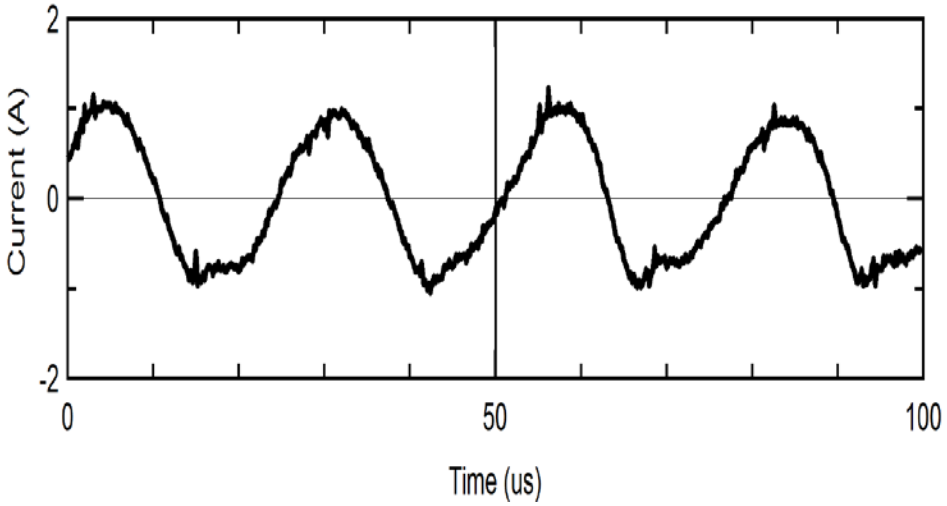


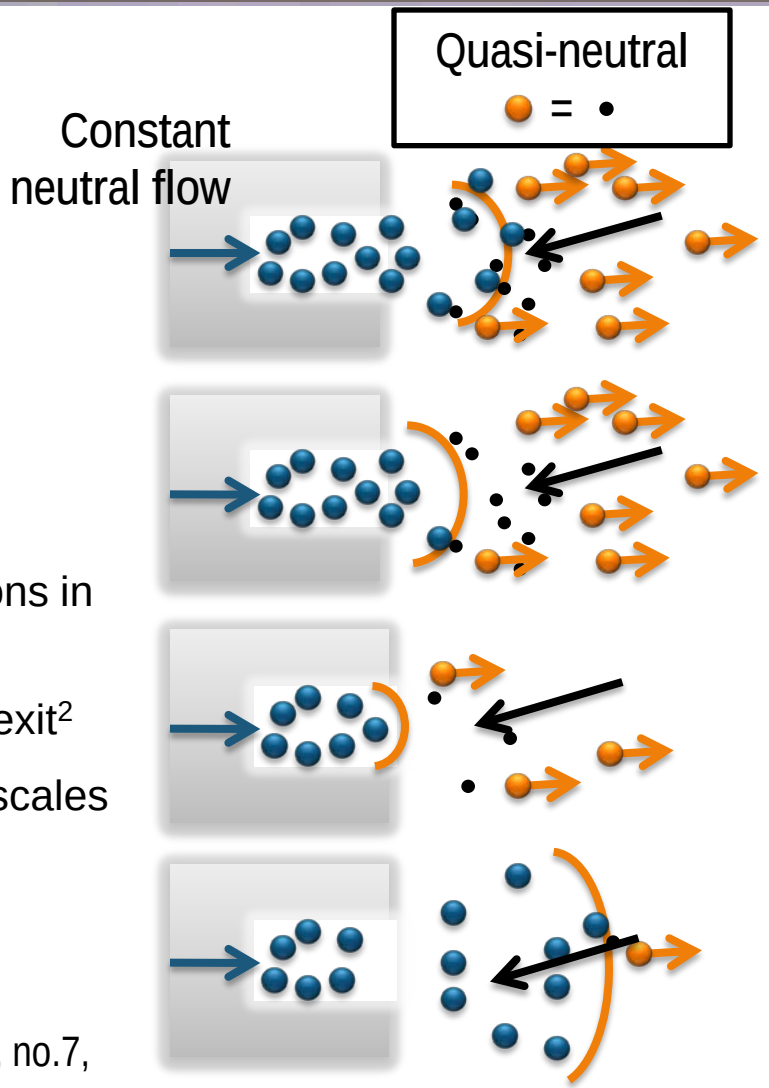


- Seen through low frequency (10-50k Hz) oscillations in discharge current ($I_d$)
- Periodic depletion & replenishment of neutrals at exit[2]
- Also referred to as neutral transit time instability- scales with $L_{channel}\ /V_{neutrals}$
- Previous time averaged measurements unable to quantify oscillations in plasma properties

[2] Boeuf, J. P.; Garrigues, L. , *Journal of Applied Physics* , vol.84, no.7, pp.3541-3554, Oct 1998

# Collisional Radiative Modeling (CRM)

- **Predicts emission by modeling collisional excitation and allowed radiative decay paths**
- **KCD³ Metastable Modeling**
  - Treated as virtual ground
  - Assumed in equilibrium

**Simplified KCD Diagram**

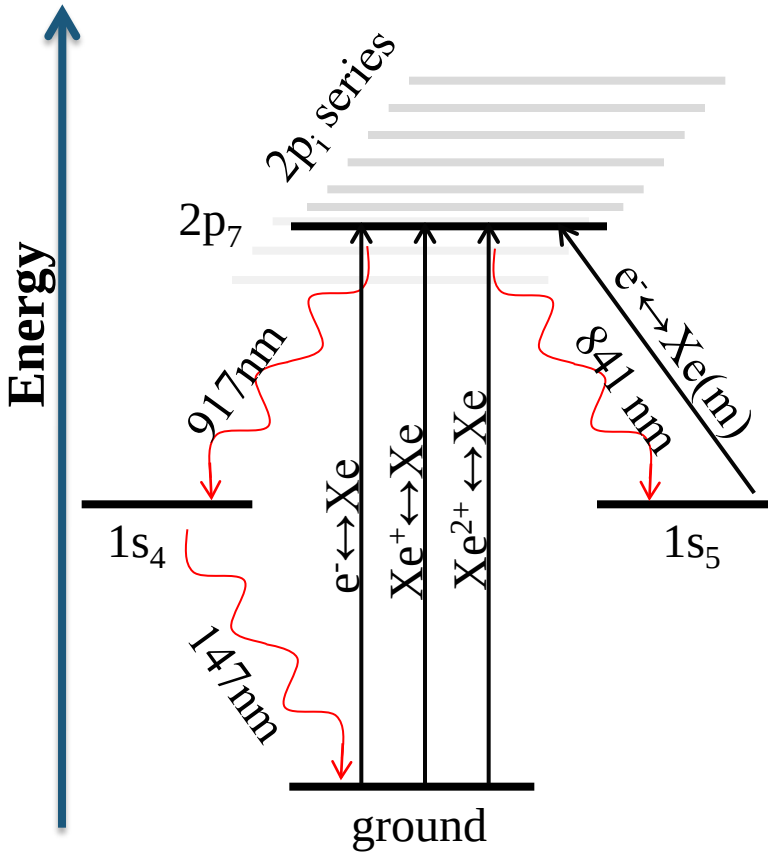


**Simplified Xe Collisional Excitation Processes**

$$e^- + Xe \rightarrow Xe^* + e^-$$
$$Xe^+ + Xe \rightarrow Xe^* + Xe^{+*}$$
$$Xe^{2+} + Xe \rightarrow Xe^* + Xe^{2+*}$$
$$e^- + Xe_m \rightarrow Xe^* + e^-$$

[3] Karabadzhak et al., *Journal of Applied Physics* , 2006

# CRM: KCD Model

$$J_{XeI}(\lambda) = \frac{hc}{4\pi\lambda}(N_0 N_e)\left[k_{eO}^{\lambda} + \frac{N_m}{N_0}k_{em}^{\lambda} + \alpha\, k_{10}^{\lambda} + \frac{1-\alpha}{2}k_{20}^{\lambda}\right]$$

$$k_{ij}^{\lambda} = \int_0^{\infty} f_i(E_i)\sigma_{ij}^{\lambda}(E_i)u_i\, dE_i$$

- **Collisional excitation rates**
  - Ground- experimental cross-sections by Chiu et al.[4] & Sommerville et al.[5]
  - Metastable- excitation approximated using 2pi degeneracy & branching probabilities
- **Energy Distribution Functions (EDF)**
  - Ions- assumed uniform velocity, velocity estimated using LIF data
  - Electrons- assumed Maxwellian EDF, function of $T_e$
- **Ratio of intensities= f($T_e$), remove dependence on $N_0$ and $N_e$**

[4]Chiu et al, *Journal of Applied Physics* , 2006.

[5] Sommerville et al, *Journal of Prop. & Power*, 2008.

# CRM: KCD Model

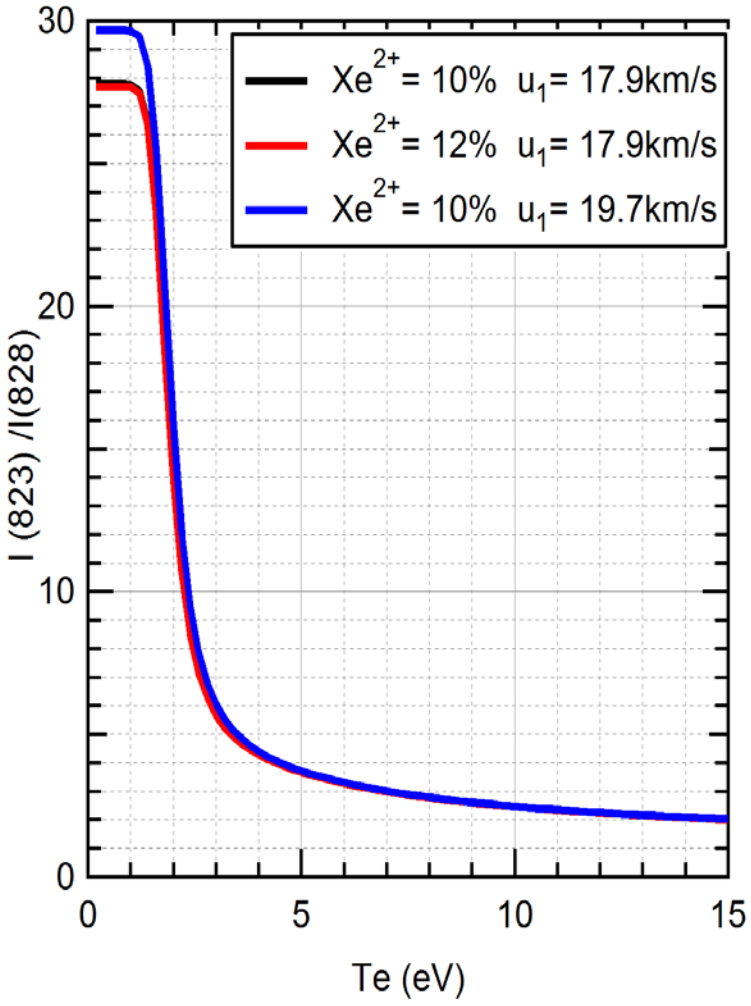


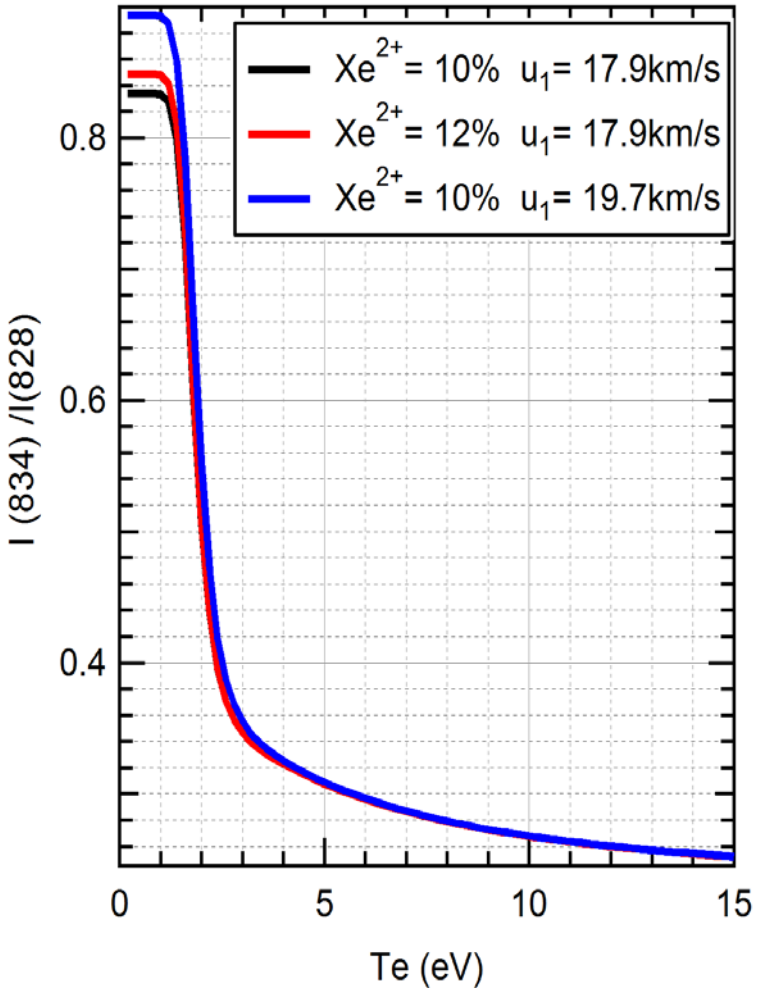

# BHT-600 Hall Effect Thruster

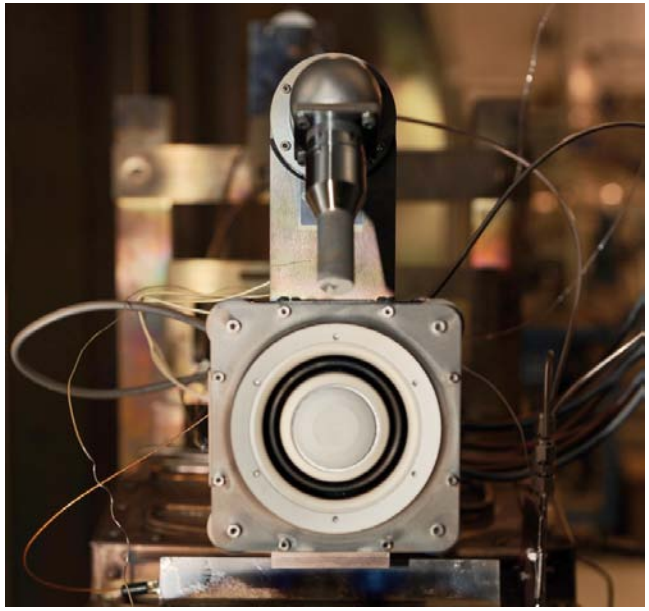

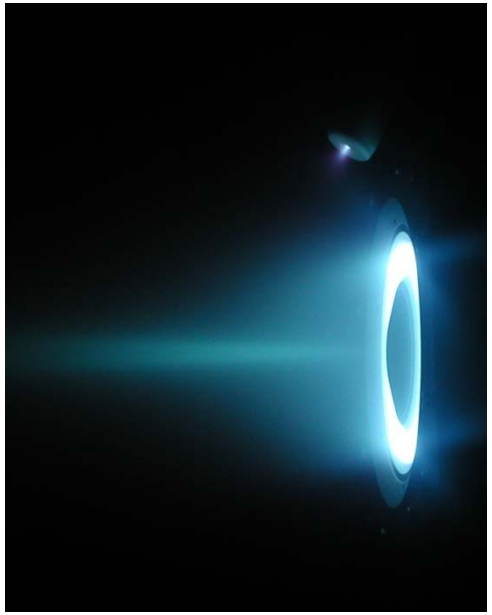

BUSEK

## Dimensions

| | |
|---|---|
| $R_{inner}$ | 24 mm |
| $R_{outer}$ | 32 mm |
| Channel Depth | 10 mm |

## Nominal Conditions

| | |
|---|---|
| Anode Flow Rate | 2.45 mg/s |
| Cathode Flow Rate | 197 μg/s |
| Anode Potential | 300 V |
| Anode Current | 2.05 A |
| Magnetic Current | 2.0 A |

## Performance

| | |
|---|---|
| Thrust | 42 mN |
| Specific Impulse | 1650 s |
| Anode Efficiency | 55.0% |

- **Thruster tested w Xe at nominal conditions**
- **Extensive previous experimental work**
  - Probe- RPA, Faraday, ExB[6-9]
  - Optical measurements-LIF[9,10],


[6] Ekholm et al, *JPC,* 2006.
[7] Niemela et al, *JPC,* 2006.
[8] Nakles et al, *IEPC,* 2009.
[9] Hargus et al, *JPC,* 2008.
[10] Nakles et al, *JPC,* 2008.

# BHT-600 Hall Effect Thruster

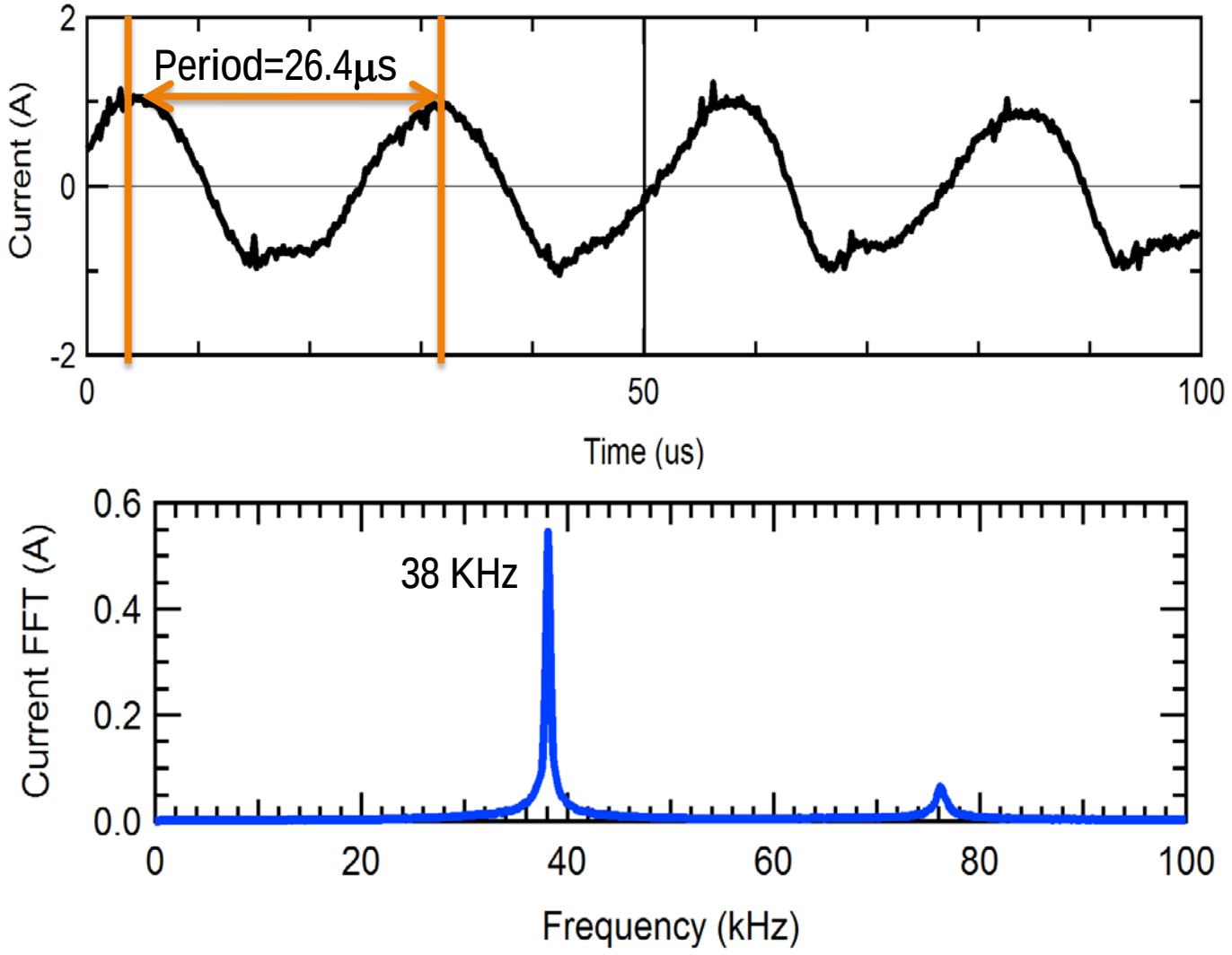

# Test Facility

## Chamber 1, AFRL Edwards AFB

- **Two cryogenic pumps**
  - 1.2 m dia., LN2 baffled (70 K), 2 stage He (15 K)
  - Pump speeds: 48,500 L/s
  - BHT-600 operation background pressure: $9.1\times10^{-6}$ Torr
- **Stainless steel chamber walls**
  - 2.4 m dia., 4.1 m length
  - Carbon beam dump
  - Flexible 1.8 mm graphite wall covering

# System Schematic

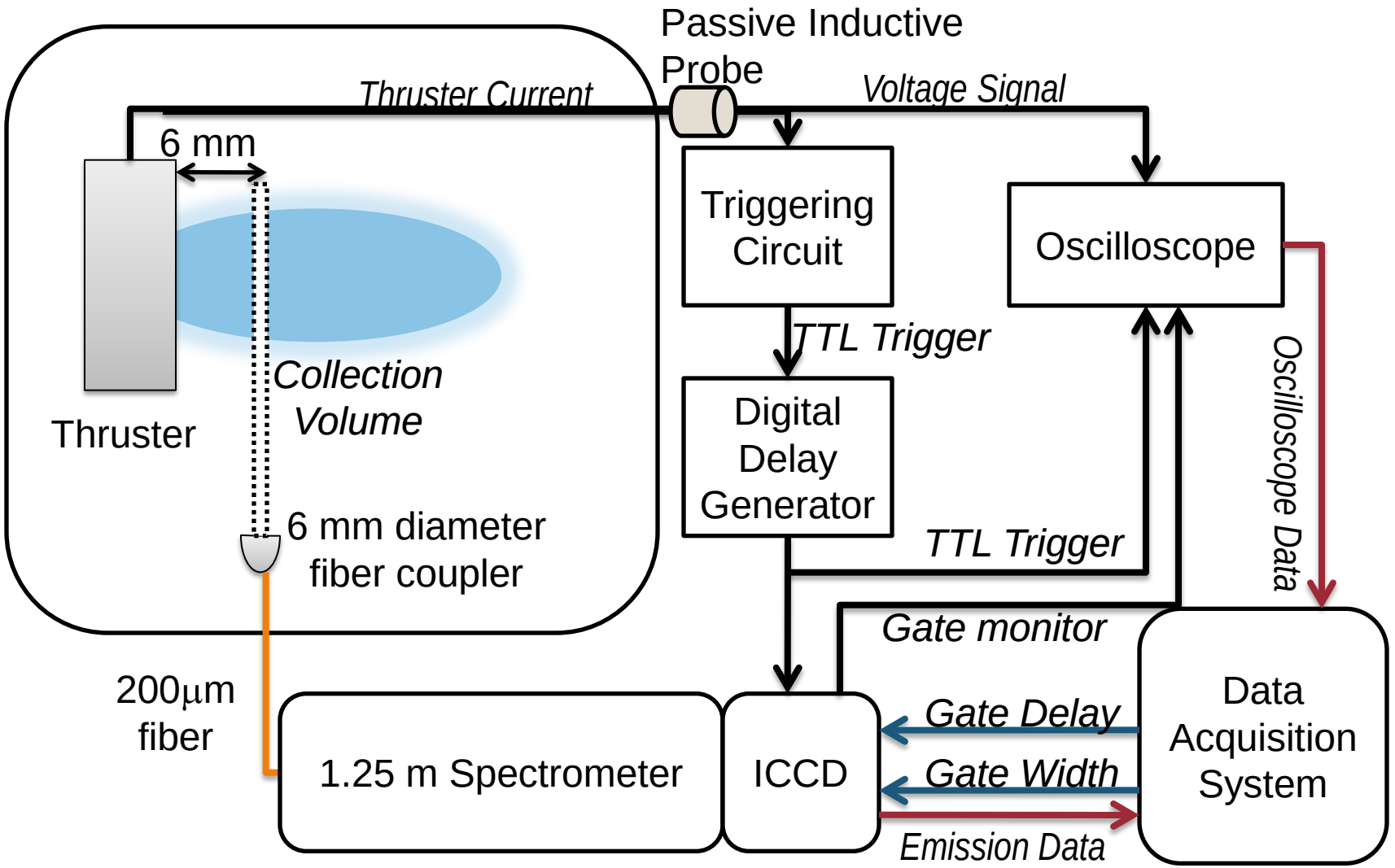

# Timing System

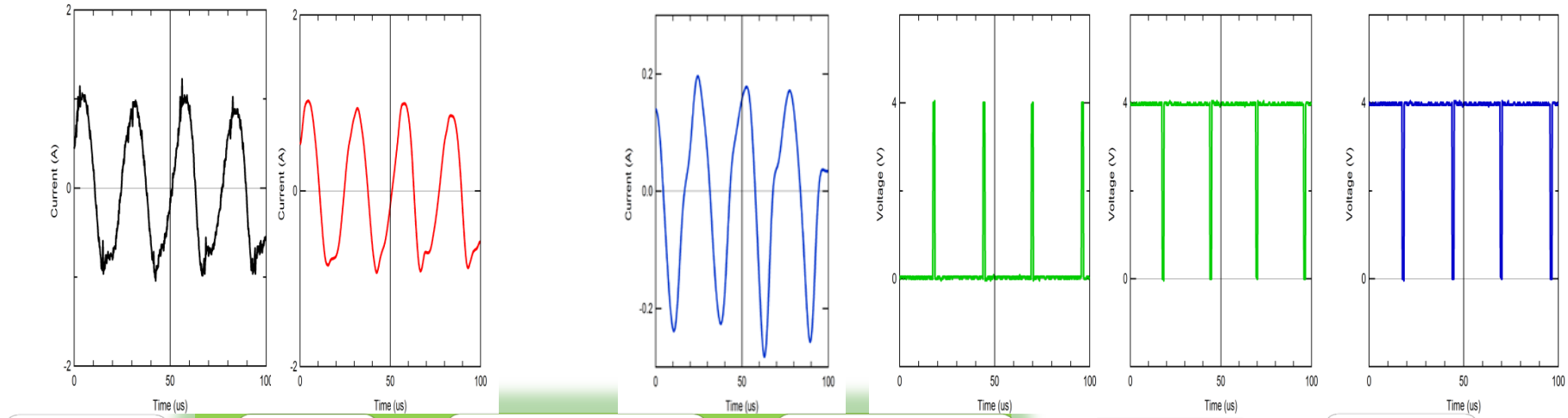


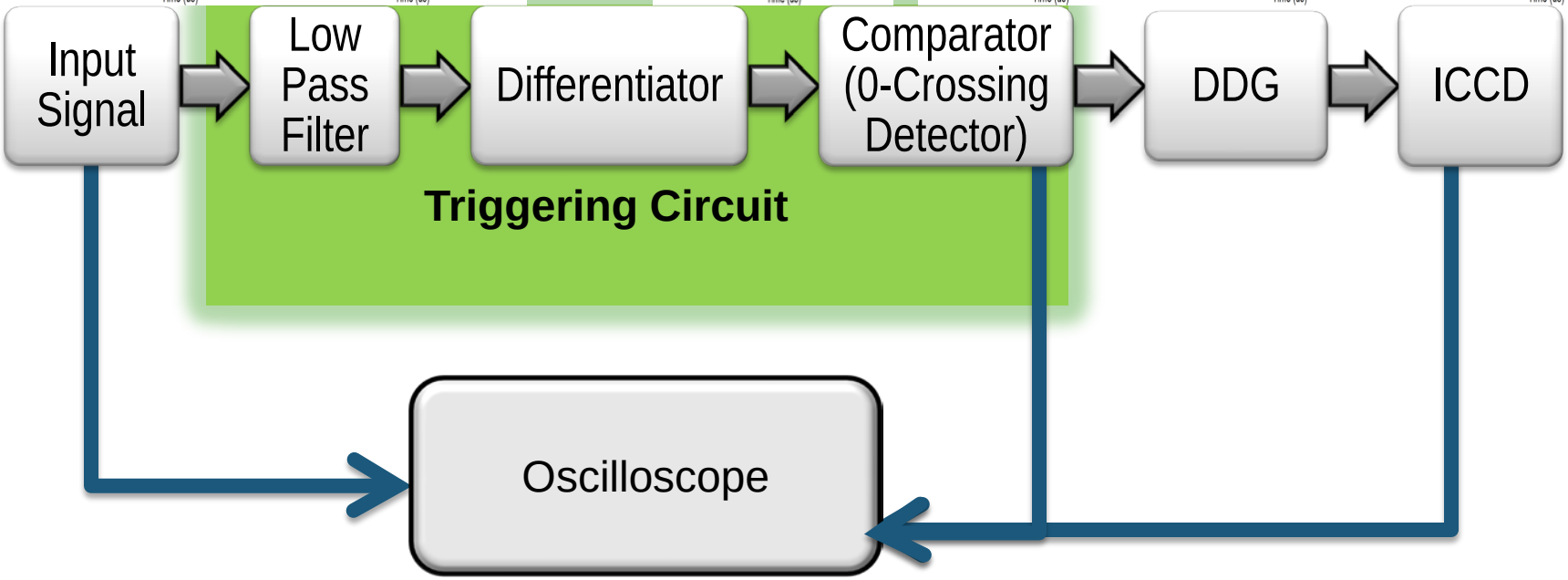

# Timing System

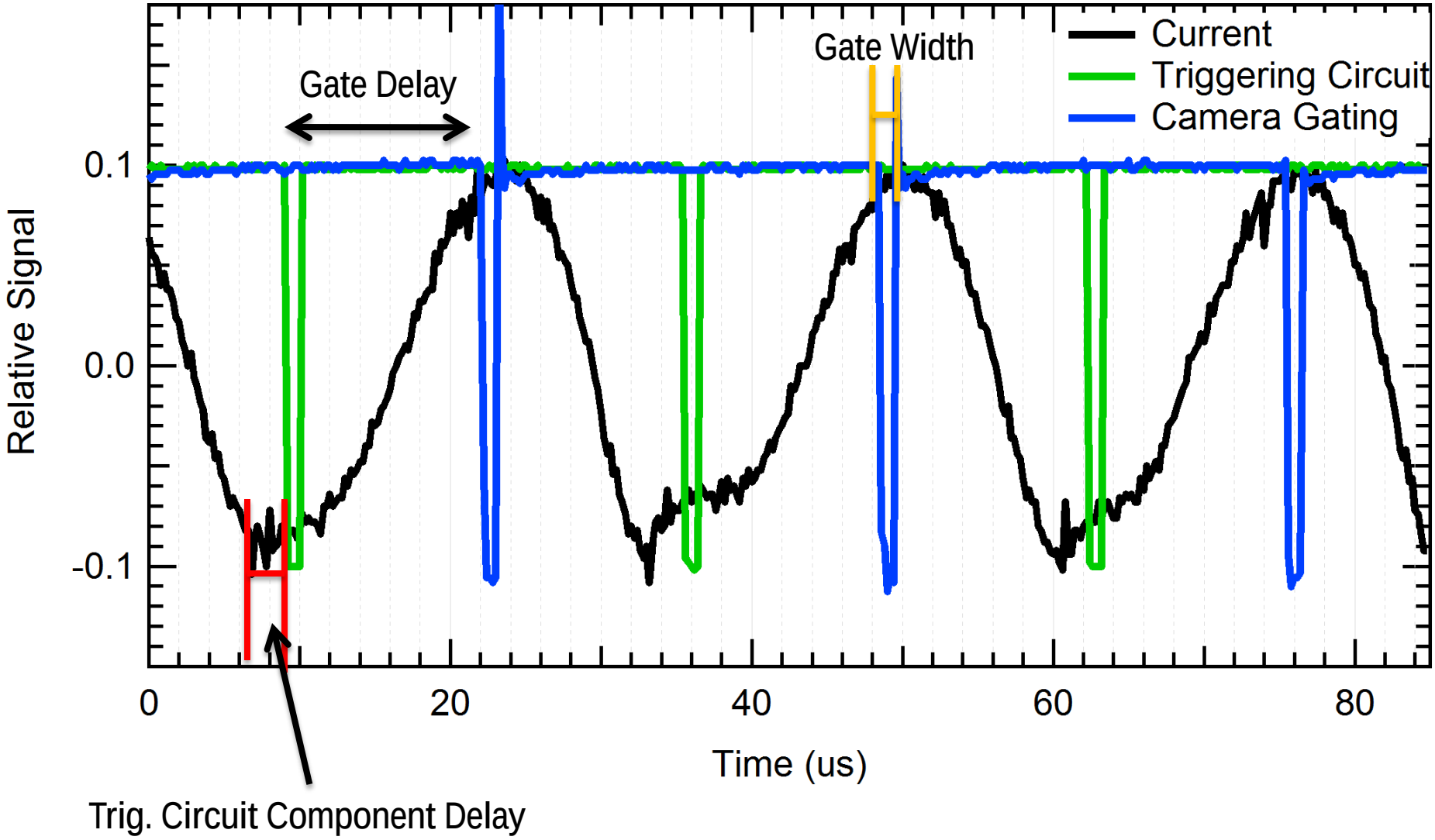

# Emission Measurements

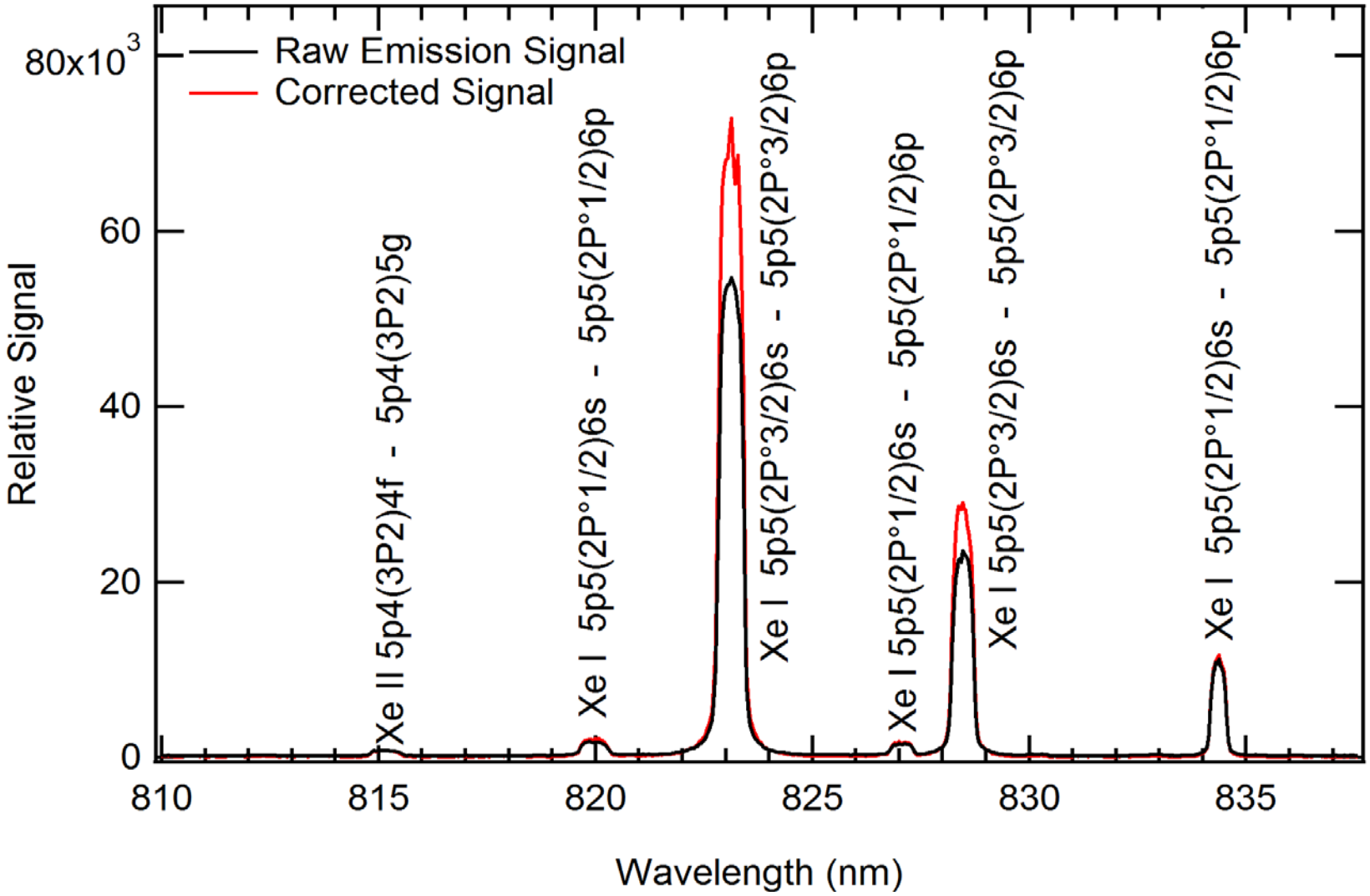

# Emission Measurements

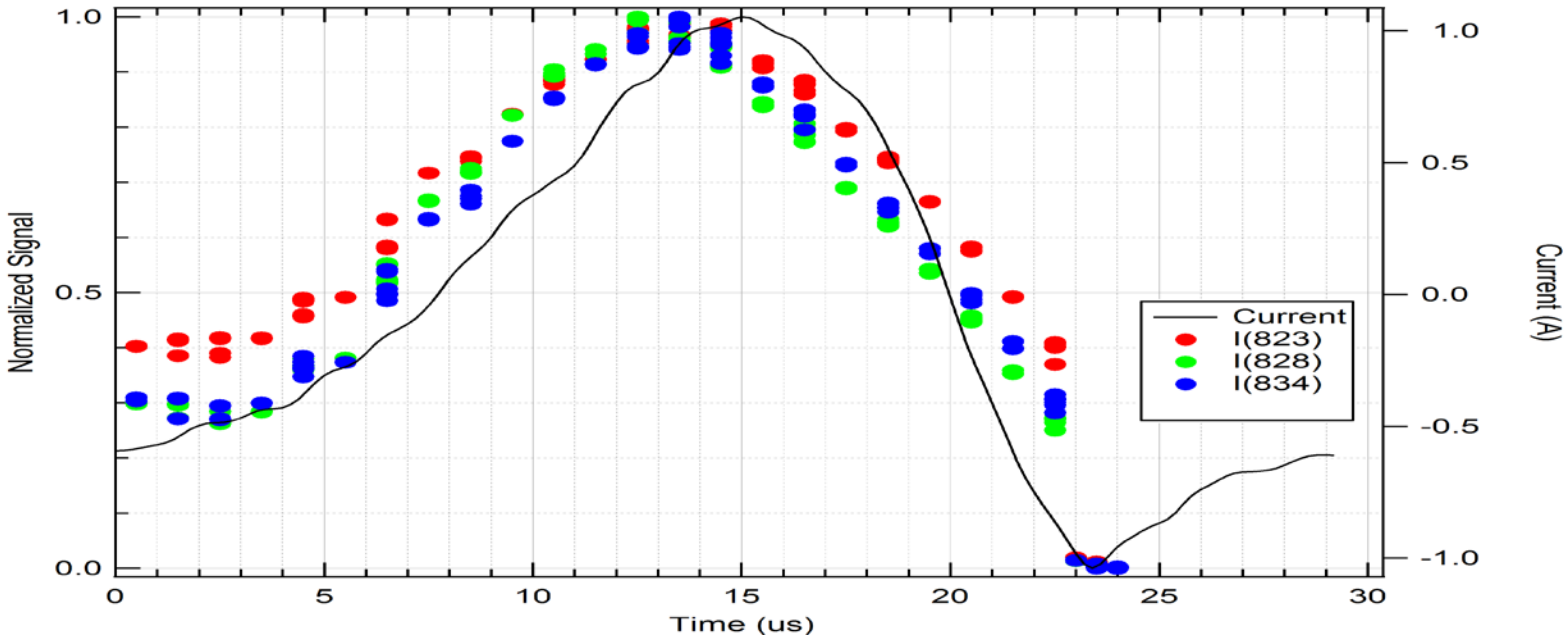


- **Intensity in phase with discharge current oscillations**
- **Similar results seen in high speed imaging by Liu et al.[11] studying visible emission fluctuations**
- **Small phase shift (~2 μs) seen between intensity and current**
  - Corresponding to a 8 km/s electron axial velocity
  - In agreement with 5-10 km/s electron axial velocity predicted by HPHall[12]


[11] Liu et al., *IEEE T. Plasma. Sci.*, (in press)

[12] Scharfe, Michelle K, Koo, Justin W, personal communication, 2011

# Electron Temperature

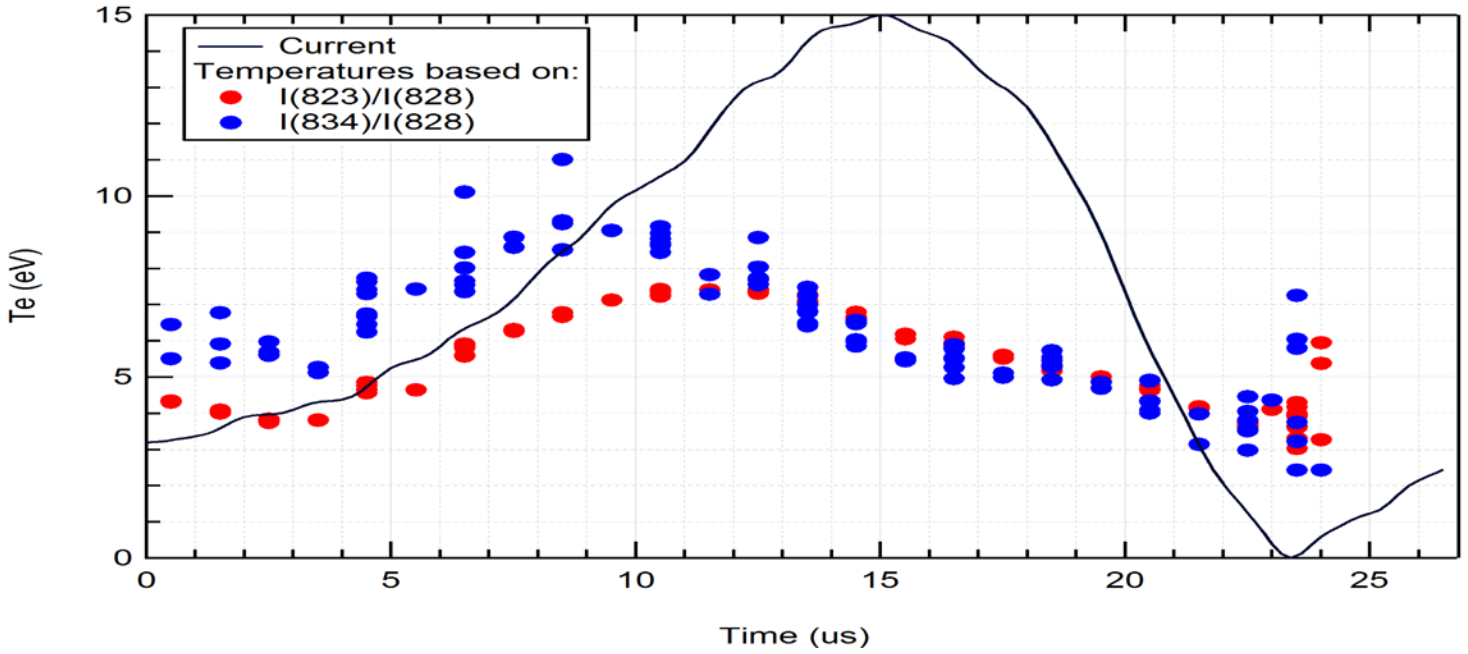


- **Line Ratio Method Disagreement may be due to :**
  - Issues with metastable approximations in that region of the cycle
  - Non-Maxwellian electron distribution
- **$T_e$ found to fluctuate between 3-10 eV, 3-6 μs out of phase with $I_d$**
  - Additional modeling needed to determine which heating/cooling mechanisms are causing this behavior

# Future Work

- **Abel inversion method[13]**
  - Vertical measurement sweeps, $T_e(y)$, transformed into $T_e(r)$

$$b(y) = 2\int_{r=y}^{r=R} f(r)dx = 2\int_{y}^{R} f(r)\frac{r}{\sqrt{r^2 - y^2}}dr$$

$$f(r) = -\frac{1}{\pi}\int_{r}^{R} \frac{b'(y)}{\sqrt{y^2 - r^2}}dy$$

- **Full plume characterization, $T_e$ (r,z,t)**
  - 5 fiber bundle coupled to spectrometer, simultaneous axial measurements
  - Use with Able inversion method to fully spatially characterize plume

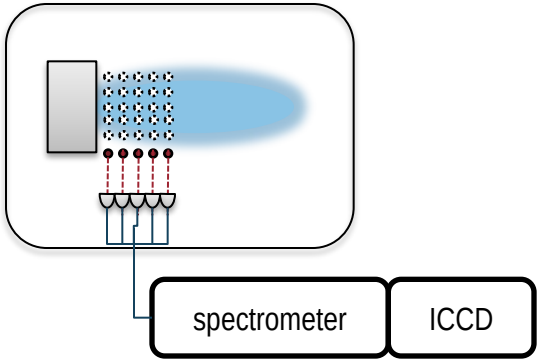


- **Compare with far field probe measurements**
- **Demonstrate applicability to other spectroscopy techniques**
  - Time resolved ion velocity measurements using Doppler shift

$$\Delta\lambda = \mp\frac{v}{c}\lambda$$

[13] Matlock, T. ; Larson, C. W. ; Hargus, WA; Nakles, MR., *JPC,* 2007

# Summary

- **Demonstration of time-resolved (1μs) non-intrusive $T_e$ diagnostic**
- **Nominal conditions of the BHT-600 produced 3-10 eV fluctuations in $T_e$ 6 mm downstream of the thruster exit plane**
- **Intensity of NIR Xe I lines found to be in phase with discharge current**
  - 2 μs delay associated with electron transit time to anode
- **Disagreement between methods for portion of cycle may indicate:**
  - More work is needed with the KCD model metastable approximations
  - An non-Maxwellian electron EDF
- **Future work focused on achieving full characterization of plume, temporally and spatially as well as expanding to other spectroscopy diagnostics**